Journal of Sound and Vibration (2002) **254**(2), 269–295
doi:10.1006/jsvi.2001.4074, available online at http://www.idealibrary.com on IDEAL®

THE ENERGY MOBILITY

G. Orefice, C. Cacciolati and J. L. Guyader

Laboratoire Vibrations Acoustique, Institut National des Sciences Appliquées, 20 *Avenue Albert Einstein,* 69621 *Villeurbanne Cedex, France. E-mail: caccio@lva.insa-lyon.fr*

(*Received* 23 *September* 1999, *and in final form* 8 *October* 2001)

The energy mobility method is presented and applied both numerically and experimentally to thin plates of high modal density. The energy mobility is defined as the ratio of the frequency averaged quadratic velocity at one point of a structure to the frequency averaged active power injected at one point of the structure. It can be calculated using only classic input and transfer mobilities. The property of energy additivity of the contributions of several external loads is shown to be a good approximation in the case of a single structure. To quantify the approximations on typical structures one is interested in, numerical simulations are presented on plates. A good agreement is found between the predictions using the energy mobility and the exact calculations. An experiment conducted on a plate with a real excitation confirms that the prediction of the energy mobility approach can be quite satisfactory. Finally, a remarkable property for the energy mobility (contrary to standard mobility) is noted: the insensitivity to the presence of a mass heterogeneity at driving points. This property allows one to simplify considerably the characterization of industrial structures that have in general a lot of heterogeneities. The energy mobility concept is further applied to the vibrational behaviour of an assembly. For each subsystem the connection is described by adding injected power and coupling power into the energy additivity. The equality of the frequency averaged quadratic velocity and the power flow balance at each coupling point allows one to calculate the coupling power at connection points with energy mobilities of uncoupled subsystems. A system of two plates has been used to compare the energy mobility calculation and the exact one given by the classic mobility method. The comparison shows that a connectivity factor must be introduced to keep the same formalism generally used with classic mobilities. A generalized definition for the energy mobility is then established.

1. INTRODUCTION

Theoretical approaches like finite elements, waves, modal calculations, or experimental ones, like modal analysis, mobilities or transfer path analysis, often cannot help to handle industrial structures which present large variations in their properties in spite of their "identical appearance" [1, 2]. Energy and average based approaches produce quantities that vary less, they are therefore more convenient to describe such groups of structures. In this way, energy methods based on substructuration are easier to use for industrial applications, like SEA for example. However, SEA does not use only the dynamic characteristics of each separate substructure, and needs a highly skilled know-how to distinguish weak coupling conditions.

The approach presented in this paper has two goals: firstly, to use local quantities that can be simply measured on the isolated substructures, as mobilities, secondly, to deal with frequency averaged energy quantities like quadratic velocities and injected powers, in order to get a robust approach as done in SEA.

0022-460X/02/$35.00

The mobility was used in reference [3] to calculate the power injected by a pure tone excitation in a single structure. To consider a broadband excitation, a force with constant amplitude was usually considered in the frequency band. So, the input power was related to the integral of the real part of the input mobility. Several authors, working on SEA, used the mobility to get a general formulation of the coupling loss factors, see for instance references [4–7]. With quite the same scope, always using mobilities, Wang and Koss [8] defined the frequency response for power (FRFP), relating the input power to quadratic velocity at one point of a structure. In a following paper [9], the FRFP for the subsystems coupled in a single point was obtained by using the FRFP defined on two uncoupled subsystems. An application was made in the case of two coupled beams.

To obtain averaged values of energy and power it is possible to do frequency or space averaging. Space averaging was introduced to smooth quantities (see references [10–12]), it is of common use in room acoustics, but this concept will not be used here, as we want to describe local behaviour.

Frequency averaging was also often used (see for example references [13–15]). Skudrzyk [16] demonstrated that the input mobility of an infinite system is equal to the geometrical mean in a frequency band of the input mobility of the same system with finite extent. In SEA-related papers (see for example references [5, 6]) frequency averages were often taken to simulate an ensemble over a class of similar structures. In this paper some frequency averaging of functions will be done. These functions are summations of fluctuating terms (which become positive and negative in the frequency band), and non-fluctuating ones. We will use the arithmetical mean over a frequency band, only in order to neglect the average of fluctuating terms when compared to the average of non-fluctuating ones. Finally, it will be possible to obtain good approximations of averaged values with simple expressions.

The study presented in this paper relates the frequency averaged quadratic velocity at a point of an assembly to the frequency averaged active injected powers at several points. Only energy mobilities of uncoupled subsystems in addition to connectivity factor are necessary to do the calculation. The method and its necessary assumptions are presented and investigated, both numerically and experimentally. The purposes of this paper are threefold: firstly, define the energy mobility; secondly, study energy additivity in the case of several excitations and thirdly, develop energy connectivity between subsystems.

2. ENERGY MOBILITY

2.1. CLASSIC MOBILITIES

The formalism is well known (see references [17, 18]) but it is useful to summarize shortly the basis of the method, because we will often refer to it in the following pages.

Let us consider a linear vibrating structure, harmonically driven by external stationary forces at angular frequency ω. For the sake of simplicity, the time dependence $e^{j\omega t}$ will be omitted in the following expressions. The mobility method is here developed for force excitations and translation velocities only, but the same formalism applies for moments and angular velocities. The external force F_n applied at point n is related to the velocity V_m resulting at point m through the mobility Y_{mn} defined as the complex ratio

$$Y_{mn} = V_m/F_n. \tag{1}$$

In the case of Ne applied forces F_e at points e the velocity produced at point m can be written, by using the linearity of the system, as the superposition of the different velocities

created by each force:

$$V_m = \sum_{(e=1,Ne)} Y_{me} F_e. \tag{2}$$

Note that the additivity of forces contributions (using relation (2)) also needs the assumption that each force excitation does not vary when other driving forces are simultaneously applied.

2.2. DEFINITION

In analogy to the classic mobility let us introduce a ratio between a quantity which characterizes the energy of the movement and a quantity which characterizes the power of the load; both quantities are averaged over a given frequency band.

Let us firstly replace the velocity V_m at a point m by the frequency averaged quadratic velocity, called FAQV, noted $\langle |V_m|^2 \rangle$, where the symbols "$\langle\ \rangle$" indicate the average over a frequency band. In the same way let us replace the force F_e by the frequency averaged active power injected at point e, called FAP and noted $\langle \Pi_e \rangle$. The ratio R_{me} is defined as

$$R_{me} = \langle |V_m|^2 \rangle / \langle \Pi_e \rangle. \tag{3}$$

Both numerator and denominator can be expressed in terms of classic mobilities of the structure by using the equations

$$\langle |V_m|^2 \rangle = \langle |Y_{me} F_e|^2 \rangle, \tag{4}$$

$$\langle \Pi_e \rangle = \langle \mathrm{Re}\{F_e V_e^*\} \rangle = \langle |F_e|^2\ \mathrm{Re}\{Y_{ee}\} \rangle. \tag{5}$$

Let us further write equation (3) in the form

$$R_{me} = \langle |Y_{me}|^2 |F_e|^2 \rangle / \langle |F_e|^2\ \mathrm{Re}\{Y_{ee}\} \rangle. \tag{6}$$

Looking at equation (6) one can see that R_{me} depends on the applied force spectrum and is not exclusively related to the structure.

For white noise excitation, the spectrum of the force F_e has a constant level over the frequency band of calculation, and thus expression (6) can be reduced to

$$R_{me} = \langle |Y_{me}|^2 \rangle / \langle \mathrm{Re}\{Y_{ee}\} \rangle. \tag{7}$$

Written in this form the ratio R_{me} just depends on the structure. The case of white noise is very particular, and not realistic in several situations. A less restrictive assumption can be made, based on the statistical independence between frequency distributions of force and mobility spectra. This assumption corresponds to the approximation of numerator and denominator of equation (6) by the relations, respectively,

$$\langle |Y_{me}|^2\ |F_e|^2 \rangle \approx \langle |Y_{me}|^2 \rangle \langle |F_e|^2 \rangle, \tag{8}$$

$$\langle |F_e|^2 \mathrm{Re}\{Y_{ee}\} \rangle \approx \langle |F_e|^2 \rangle \langle \mathrm{Re}\{Y_{ee}\} \rangle. \tag{9}$$

Relation (8) assumes a statistical independence between the frequency distribution of the input force modulus squared and the frequency distribution of the mobility modulus squared. Relation (9) assumes statistical independence between frequency distribution of the input force modulus squared and of the real part of the input mobility. The validity of these assumptions will be tested in section 5, in the case of a plate excited with different kinds of input forces.

By making use of relations (8) and (9) the ratio R_{me} can be approximated again by equation (7), expressed exclusively in terms of structure characteristics and so does not depend on the excitation. We define then the energy mobility H_{me} as the ratio

$$H_{me} = \langle |Y_{me}|^2 \rangle / \langle \mathrm{Re}\{Y_{ee}\} \rangle. \tag{10}$$

Thus, the energy mobility H_{me} is an approximation of the ratio FAQV/FAP, valid when the previous assumptions of statistical independence are correct. It appears as a generalization for broadband excitation of the classical expression (11a) given in reference [3] for pure tone excitation:

$$|V_m|^2 / \Pi_e = |Y_{me}|^2 / \mathrm{Re}\{Y_{ee}\}. \tag{11a}$$

The frequency response function for power (FRFP), introduced in reference [8], coincides also with equation (11a) for pure tone excitation. But in the case of band-limited excitation FRFP (expression (11b)) is different for energy mobility.

$$\langle |V_m|^2 \rangle / \langle \Pi_e \rangle = \langle \mathrm{Re}\{Y_{ee}\} |Y_{me}|^2 \rangle / \langle (\mathrm{Re}\{Y_{ee}\})^2 \rangle. \tag{11b}$$

Of course there is an obvious link between FRFP and energy mobility; they coincide when statistical independence of $\mathrm{Re}\{Y_{ee}\}$ and $|Y_{me}|^2$ frequency distribution prevails.

In the following pages the energy mobility defined by relation (10) will be called EMo; it locally characterizes the structure and does not depend on the external source.

Note that, unlike, the classic mobility matrix that is symmetric, the energy mobility matrix is non-symmetric. For heterogeneous structures, classic input mobility can strongly vary from one point to another one, implying a large non-symmetry for the EMo matrix: $H_{me} \neq H_{em}$.

3. THE ENERGY ADDITIVITY

Using several loads, in reference [19] and more recently reference [12] the calculation of the input power on a multi-port system was studied. These studies introduce the concept of mean effective impedance and mean effective mobility, resulting from a spatial averaging of the input impedance or mobility. However, the assumption of a uniform distribution of forces on each excited point is necessary and the equivalent source defined in this way can be unrealistic when the phase of the excitation is still needed. Furthermore, in our case the concept of identical input forces is not acceptable because the aim of the study is to describe the coupling between subsystems.

Let us first perform the exact calculation of FAQV using classic mobilities. The FAQV at point m due to N_e driving forces located at points e, can be written by using equation (2) as

$$\langle |V_m|^2 \rangle = \langle |\textstyle\sum_{(e=1,Ne)} Y_{me} F_e|^2 \rangle. \tag{12}$$

Equation (12) can be developed as follows, where e and f are indices of driving point forces:

$$\langle |V_m|^2 \rangle = \textstyle\sum_{(e=1,Ne)} [\langle |Y_{me} F_e|^2 \rangle + 2 \sum_{(f>e)} \langle \mathrm{Re}\{Y_{me} F_e Y_{mf}^* F_f^*\} \rangle]. \tag{13}$$

The frequency averaged injected power at points e can be written as

$$\langle \Pi_e \rangle = \langle \mathrm{Re}\{F_e V_e^*\} \rangle = \langle \mathrm{Re}\{F_e \textstyle\sum_{(f=1,Ne)} Y_{ef}^* F_f^*\} \rangle. \tag{14}$$

As for equation (12), a developed expression can be obtained. The input power at point e can then be expressed as

$$\langle \Pi_e \rangle = \langle \mathrm{Re}\{Y_{ee}\}|F_e|^2 \rangle + \sum_{(e,f>e)} \langle \mathrm{Re}\{Y_{ef}^* F_e F_f^*\} \rangle. \tag{15}$$

Let us now remark that the first terms of equations (13) and (15) are averages over frequency of positive quantities. On the contrary, the second terms are averages over frequency of fluctuating quantities (which become positive and negative within the frequency band). Consequently, the frequency average renders the fluctuating terms' contribution small compared to that of the non-fluctuating ones in equations (13) and (15). The two following assumptions are based on this fact:

$$\langle |Y_{me} F_e|^2 \rangle \gg 2 \sum_{(f>e)} \langle \mathrm{Re}\{Y_{me}\ F_e Y_{mf}^* F_f^*\} \rangle, \tag{16}$$

$$\langle \mathrm{Re}\{Y_{ee}\}|F_e|^2 \rangle \gg \sum_{(e,f>e)} \langle \mathrm{Re}\{Y_{ef}^* F_e F_f^*\} \rangle, \tag{17}$$

and lead to

$$\langle |V_m|^2 \rangle \approx \sum_{(e=1,Ne)} \langle |Y_{me}|^2 |F_e|^2 \rangle, \tag{18}$$

$$\langle \Pi_e \rangle \approx \langle \mathrm{Re}\{Y_{ee}\}|F_e|^2 \rangle. \tag{19}$$

The fundamental requirement for the energy additivity in this calculation is that the transfer mobility Y_{ef} between two excited points e and f has an imaginary and a real part which oscillate (go through zero) sufficiently (at least three times in several calculations we have done) in each frequency band. This assumption can be verified while measuring or computing the classic mobilities to choose the right frequency bands for the energy mobility method. This will happen generally when the points e and f are separated by a distance larger than two wavelengths. In the situation where the mutual distance between forces is of the order of one wavelength or smaller, neglecting cross terms in equations (13) and (15) is not realistic. In the following we suppose this is not the case. Using again the previously made approximations (8) and (9) one gets the following equations (20) and (21). Equation (21) shows that the injected power at each excited point is not dependent on the other input forces, and finally, equation (22) establishes the energy additivity property:

$$\langle |V_m|^2 \rangle \approx \sum_{(e=1,Ne)} \langle |Y_{me}|^2 \rangle \langle |F_e|^2 \rangle, \tag{20}$$

$$\langle \Pi_e \rangle \approx \langle \mathrm{Re}\{Y_{ee}\} \rangle \langle |F_e|^2 \rangle \tag{21}$$

and

$$\langle |V_m|^2 \rangle \approx \sum_{(e=1,Ne)} H_{me} \langle \Pi_e \rangle. \tag{22}$$

The validity of this expression relies on those of relations (8), (9), (16) and (17). In the case of random, broadband, uncorrelated forces, energy additivity is strictly valid. If the forces are correlated, relation (22) will still be valid if the structure mobility fluctuates enough to make equations (8), (9), (16), (17) true in a first approximation. The energy additivity (22) shows that no phase information is needed between excitations to describe the sources. Only frequency averaged powers separately injected at each input point are necessary. In the particular case of coupling forces between coupled substructures the statistical independence assumption is violated and equation (22) is not applicable. This case will be studied in sections 7 and 8 about connectivity.

4. DISCUSSION

4.1. INTRODUCTION

The goal of this section is to test numerically the validity of the assumptions one has to make to obtain the energy additivity. In a first step one can analyze the difference between the energy mobility (EMo) defined by equation (10) and the exact calculation given by equation (3), testing in this way the approximations (8) and (9) proposed in section 2. In a second step, the exact calculation of the frequency average quadratic velocity (FAQV) at a given point will be compared to the result of relation (22).

The discussion about the definition of the EMo and the validity of the energy additivity will be made on physical grounds, looking at the difference between exact and approximated results versus structure parameters like modal density, modal overlap, number of modes in the excited frequency band, etc.

One difficulty arises when conducting numerical experiments, due to the fact that results depend on the force spectra. In general, driving forces result from the interaction of the structure with external sources. Using the classic mobility result for one coupling point, one can express the driving force at point e as

$$F_e = \mathbf{V}_s/(Y_s + Y_e), \tag{23}$$

where Y_s is the output mobility of the source, Y_e is the input mobility of the structure at point e and $\mathbf{V}_s$ is the source velocity (before coupling). Two extreme cases can be defined, see for example reference [12]: the force source ($Y_s \gg Y_{ee}$) which injects always the same force F_e, and constant velocity source ($Y_s \ll Y_e$) which imposes always the same velocity $\mathbf{V}_s$ on the structure, whatever the mobility at the input point is like. The EMo approach will be tested using these two kinds of source, and a typical steel plate simply supported along its four edges (1·0 m length, 0·70 m width, 0·001 m thickness), corresponding to an asymptotic modal density equal to 0·22 modes/Hz. Two values of damping loss factor will be used in the calculation ($\eta = 0{\cdot}01$ and 0·10) in order to have plates with quite different modal overlap. Numerical results will be given for four possible points on the plates: m_1 (0·2 m, 0·5 m), e_1 (0·4, 0·2 m), e_2 (0·7, 0·3 m), e_3 (0·5, 0·6 m).

In the calculation with the constant force source a unit force spectrum level will be used; as it does not depend on the structure mobility, it is a favourable case regarding assumptions (8) and (9). However, for multiple excitation with the same amplitude and phase, the different forces are totally correlated and then constitute an unfavourable case regarding assumptions (16) and (17).

In the calculation with a constant velocity source a unit velocity spectrum level will be used. The resulting force spectrum varies with frequency, especially in the case of low damping, but its frequency distribution is directly associated to the plate mobility at the driving point and this case is unfavourable regarding assumptions (8) and (9) (statistically independent force and plate mobility spectra).

4.2. TESTING THE APPROXIMATION DONE DEFINING THE ENERGY MOBILITY

To explore numerically the limits of assumptions (8) and (9) one firstly compares the EMo given by definition (10), which depends only on the structure mobilities, to the energy ratio of equation (3), which depends also on the external loads. In equation (3), the ratio $\langle |V_m|^2 \rangle / \langle \Pi_e \rangle$ is obtained by using the exact calculation of the quadratic velocity $|V_m|^2$ and active power Π_e at each frequency and then taking frequency averages to get $\langle |V_m|^2 \rangle$ and $\langle \Pi_e \rangle$.

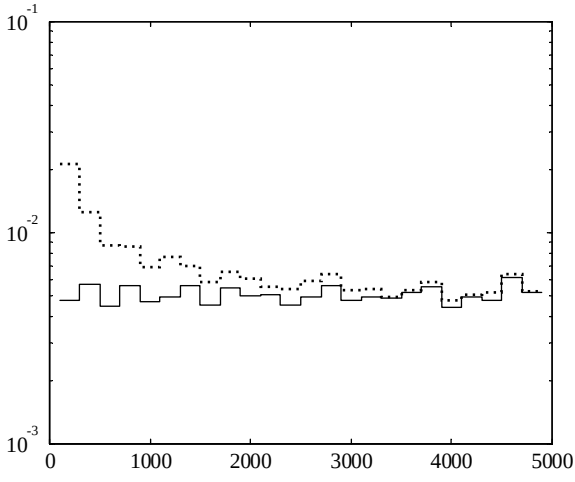

Figure 1. Input EMo (s/kg) at e_1 (0·4, 0·2 m), versus frequency; velocity source excitation, bandwidth 200 Hz, $\eta = 0{\cdot}01$. ——, Exact calculation with equation (3);……, calculation with definition (10).

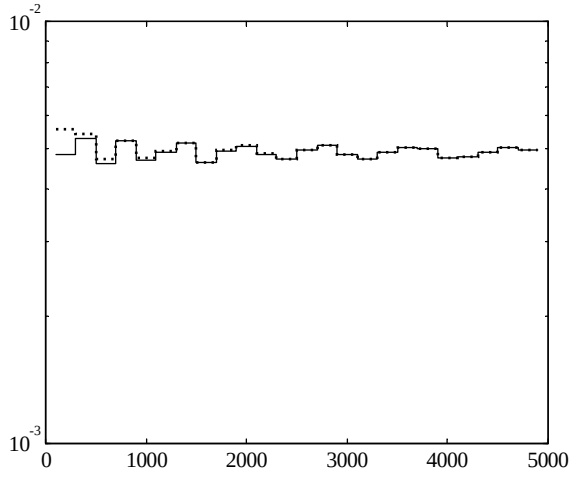

Figure 2. Input EMo (s/kg) at e_1 (0·4, 0·2 m), versus frequency; velocity source excitation, bandwidth 200 Hz, $\eta = 0{\cdot}10$. ——, Exact calculation with equation (3);……, calculation with definition (10).

As mentioned in section 2, there is no difference between the results of equations (3) and (7) when the modulus of the input force is constant over the frequency band of calculation. On the contrary, the case of a velocity source appears critical regarding the difference between the results of equations (3) and (10). In Figure 1 this comparison is done for the plate with low damping presented in section 4.1. One can observe differences up to 6 dB at 200 Hz for the input EMo but the discrepancy becomes very small at higher frequency.

Increasing the plate loss factor to 0·10 reduces considerably the differences, and as presented in Figure 2, the two curves are almost identical. To understand the underlying phenomenon, one can first remark that in the two cases the plates have the same asymptotic modal densities (the number of modes in each frequency band of 200 Hz is $\simeq 44$). Thus, the different behaviours of the two plates are not due to the modal density ($n(\omega)$) but to the

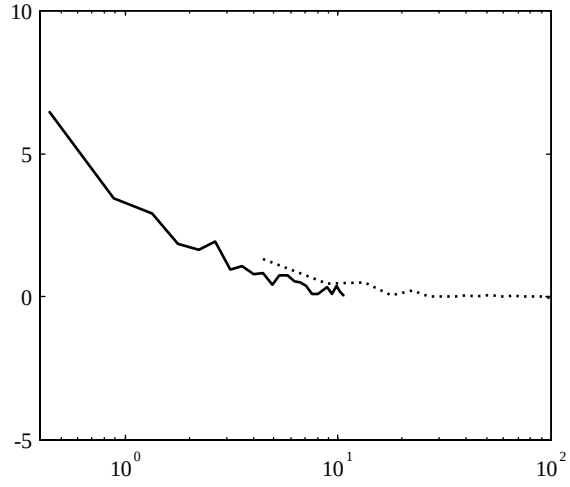

Figure 3. Error at input point e_1 (0·4, 0·2 m), versus modal overlap; velocity source excitation, bandwidth 200 Hz. Error $= 10 \log_{10}$ ($H_{e_1e_1}$ given by definition (10)/$R_{e_1e_1}$ given by equation (3)). ——, Plate with $\eta = 0{\cdot}01$;……, plate with $\eta = 0{\cdot}10$.

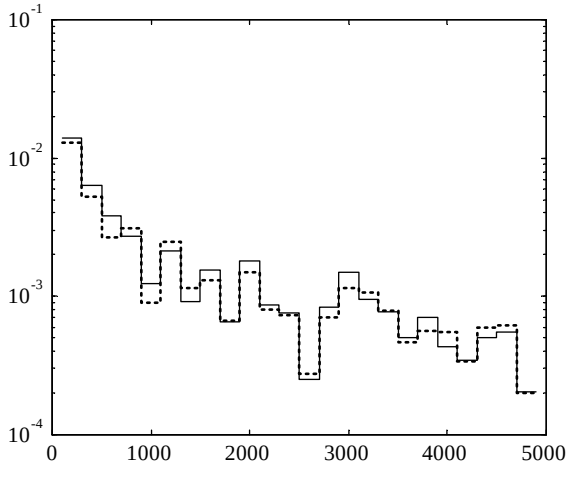

Figure 4. Transfer EMo $H_{m_1e_1}$ versus frequency; m_1 (0·2, 0·5 m), e_1 (0·4, 0·2 m); velocity source excitation, bandwidth 200 Hz, $\eta = 0{\cdot}01$. ——, Calculation with equation (3);……, calculation with definition (10).

modal overlap (m.o.) defined by equation (24), where η is the damping loss factor, and ω the frequency in rad/s:

$$m.o. = n(\omega)\eta\omega. \tag{24}$$

Figure 3 presents, for both plates, the ratio of the results of (3) and (10), plotted versus the plate modal overlap. The difference can reach 6 dB with a modal overlap equal to 0·5, it decreases to 3 dB when the modal overlap is close to 1 (for example at 500 Hz with $\eta = 0{\cdot}01$ or at 50 Hz with $\eta = 0{\cdot}1$) and becomes negligible when the modal overlap is > 4.

The physical explanation of this is that when the modal overlap increases, the plate mobility and the associated force spectrum become more and more smoothed and flat and so can be considered frequency independent in the correspondent frequency bands. Thus, it

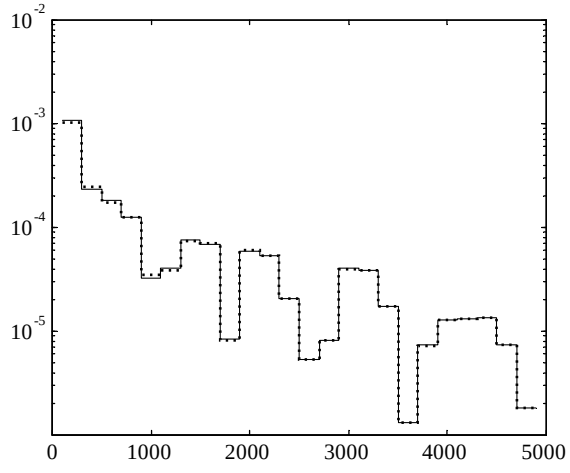

Figure 5. Transfer EMo $H_{m_1 e_1}$ versus frequency; m_1 (0·2, 0·5 m), e_1 (0·4, 0·2 m), velocity source excitation, bandwidth 200 Hz, $\eta = 0{\cdot}10$. ——, Calculation with equation (3); ……, calculation with definition (10).

appears that the parameter governing the approximation done by replacing equation (3) with equation (10), called "error within the definition for the input EMo", is the plate modal overlap.

For the transfer EMo the differences between equations (3) and (10) become considerably smaller than the previous ones as shown in Figures 4 and 5. The transfer EMo defined by equation (10) relates then correctly FAQV to FAP over all the frequency bands used. This is due to the fact that the propagation path produces the needed statistical independence between the frequency distributions of the classic transfer mobility and of the input mobility (related to the input force). The necessary distance of propagation R to produce the statistical independence is related to the vibration wavenumber k. It is achieved when $kR > 2$.

4.3. INFLUENCE OF MASS HETEROGENEITY

In industrial structures, heterogeneity is often present and renders the analysis more difficult. To simulate this effect a plate with added masses is studied. The plate defined in section 4.1 is used with three attached masses at the following points: 0·100 kg at m_1 (0·2, 0·5 m), 0·500 kg at m_2 (0·6, 0·3 m) and 0·200 kg at e_3 (0·5, 0·6 m). Three other points with no added mass are studied: e_1 (0·4, 0·2 m), e_2 (0·7, 0·3 m) and e_4 (0·4, 0·4 m). The input and transfer energy mobilities are presented in Figures 6–8 in the case of points with or without mass heterogeneity.

The classic input mobility of a plate is strongly modified at a point where a mass has been added, particularly at high frequency where its level decreases by 6 dB/Oct instead of being constant [3]. On the contrary, the input EMo at the same point remains almost unaffected by the presence of the mass (see Figure 6).

The transfer mobility is presented in Figure 7 when a mass heterogeneity is located at the input point m_2 and compared to the case of the plate without added masses. As for the input EMo, the mass has no influence on the transfer EMo when it is located at the power injection point. When the added mass is located at the receiving point, the level of the transfer EMo decreases considerably (see Figure 8).

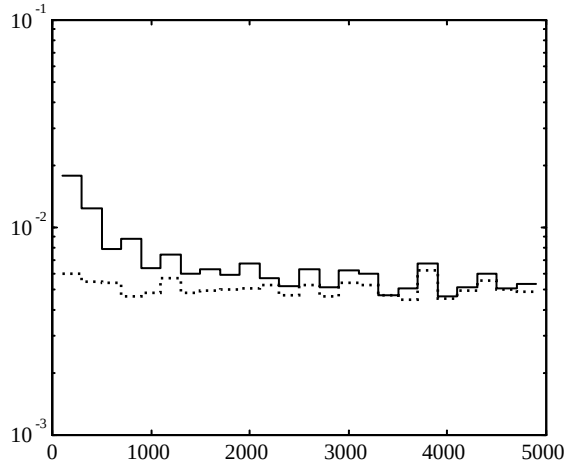

Figure 6. Input EMo on the mass loaded point m_2 versus frequency; velocity source excitation at m_2 (0·6, 0·3 m), bandwidth 200 Hz, $\eta = 0{\cdot}01$. ——, Homogeneous plate;……, Heterogeneous plate.

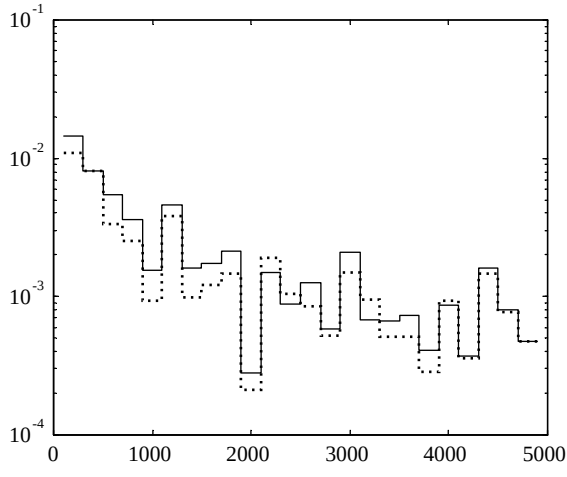

Figure 7. Transfer EMo $H_{e_4 m_2}$ versus frequency; m_2 (0·6, 0·3 m), e_4 (0·4, 0·4 m); velocity source excitation, bandwidth 200 Hz, $\eta = 0{\cdot}01$. ——, Homogeneous plate;……, heterogeneous plate.

In summary, the effect of mass heterogeneity on EMo is weak when located at the input point. This result is of considerable interest for applications to industrial structures which often have heterogeneity located around input forces.

For these structures, classic calculations using forces and displacements to study the vibration will be very sensitive to uncertainty around the heterogeneity points. On the contrary, thinking in terms of active injected power and energy mobility will give a robust description of the frequency averaged squared velocity level at every point.

4.4. TESTING THE ENERGY ADDITIVITY

The goal of this section is to check the validity of the "energy additivity property", comparing the result of the powers contributions addition of relation (22) to the exact

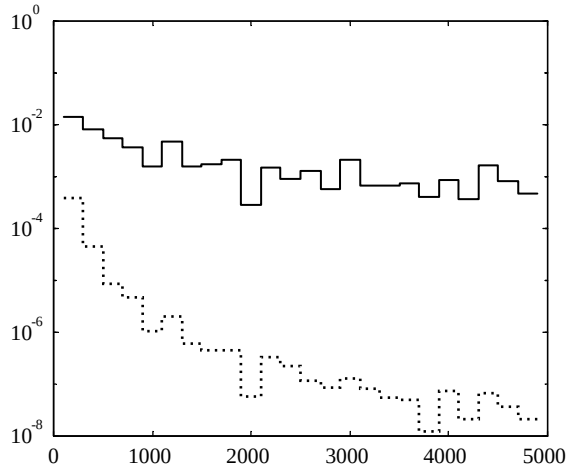

Figure 8. Transfer EMo $H_{m_2 e_4}$ versus frequency; m_2 (0·6, 0·3 m), e_4 (0·4, 0·4 m); velocity source excitation, bandwidth 200 Hz, $\eta = 0{\cdot}01$. ——, Homogeneous plate;……, heterogeneous plate.

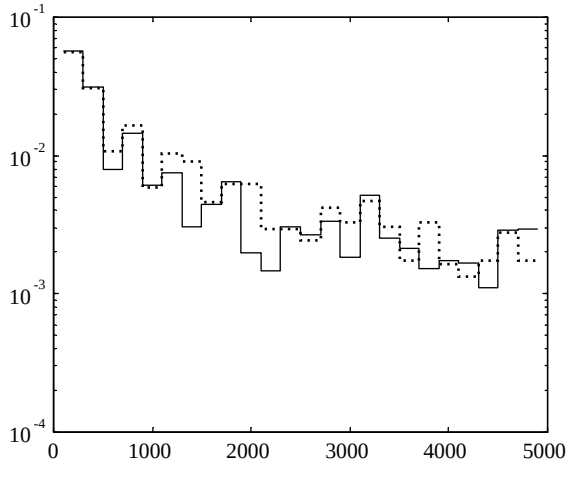

Figure 9. FAQV at the non-excited point m_1 (0·2, 0·5 m) versus frequency; three identical unit forces, bandwidth 200 Hz, $\eta = 0{\cdot}01$. ——, Exact calculation;……, calculation with definition (22).

calculation, given by equation (10). This will be done with the same plate and the two types of force spectra described in section 4.1. As previously, some forces appear as favourable cases and others as unfavourable ones; both are presented. In all the following results the plate is homogeneous and excited at three points.

In the example of Figure 9, three force sources with a constant unit spectrum in the frequency bandwidth are used. Due to the constant value of the forces, the error introduced by the definition disappears and the discrepancies between the exact result (equation (13)), and the energy additivity calculation (relation (22)) are purely associated to the additivity property. The two calculations give again similar results.

Three velocity sources defined in section 4.1 are then used to get the result of Figure 10. These force spectra are unfavourable regarding the error by the definition as demonstrated in section 4.2, but also for the addition of powers contributions because the three forces

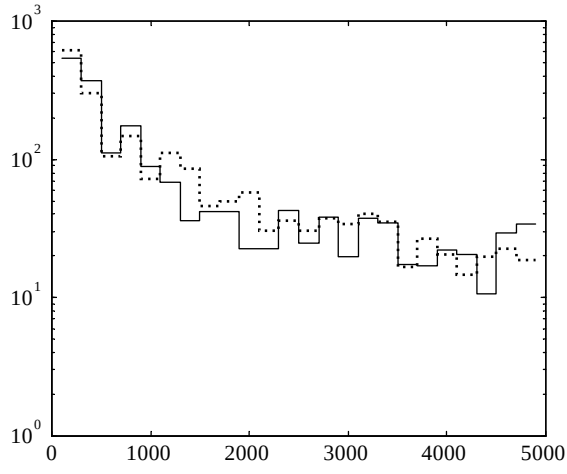

Figure 10. FAQV at the non-excited point m_1 (0·2, 0·5 m) versus frequency; three velocity sources, bandwidth 200 Hz, $\eta = 0{\cdot}01$. ——, Exact calculation;……, calculation with relation (22).

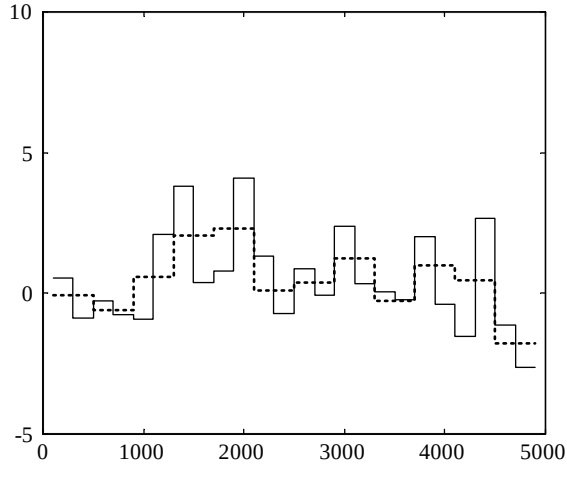

Figure 11. Error on the FAQV at the non-excited point m_1 (0·2, 0·5 m) versus frequency; error = $10\ \mathrm{Log}_{10}\ (\langle|v|^2\rangle_{\mathrm{EMo}}/\langle|v|^2\rangle_{\mathrm{EXACT}})$; three velocity sources, modal loss factor $\eta = 0{\cdot}01$. ——, Bandwidth 200 Hz;……, bandwidth 400 Hz.

depend on the mobilities of the same structure and thus, are correlated. In spite of both approximations, the difference between the exact calculation and the EMo prediction shown in Figure 10 is quite small.

4.5. INFLUENCE OF THE AVERAGING BANDWIDTH

This influence of the frequency bandwidth is presented in Figure 11. As one can see, the discrepancy between exact and EMo calculations decreases when the bandwidth of the calculation increases. This is of course consistent with the assumptions made in the EMo method that appears to asymptotically converge to the exact solution when the number of modes controlling the plate response increases.

5. EXPERIMENTAL EXAMPLES

The experimental set-up is presented in Figure 12. A rectangular steel plate (1 m × 1·2 m × 0·003 m) with two identical Plexiglas windows (0·3 m × 0·3 m) was clamped on a concrete box. The asymptotic modal density of the simply supported plate alone (without holes) is 0·126 modes/Hz. The connection between the plate and the windows was made of a standard rubber join.

Classic mobilities were measured, allowing us to calculate the energy mobilities with equation (10) over frequency bands of 200 Hz. Two experiments were done; in the first one the forces were quite uncorrelated, contrary to the second one, where correlated forces were used. In both experiments approximately the same powers were injected at points P_1 (0·3, 0·84 m) and P_2 (0·8, 0·48 m), using shakers.

Uncorrelated forces: the two input signals were provided to shakers by two independent random sources in order to produce a close level of FAP. Comparison of measured FAQV and that calculated with EMo was very good in general (see Figure 13).

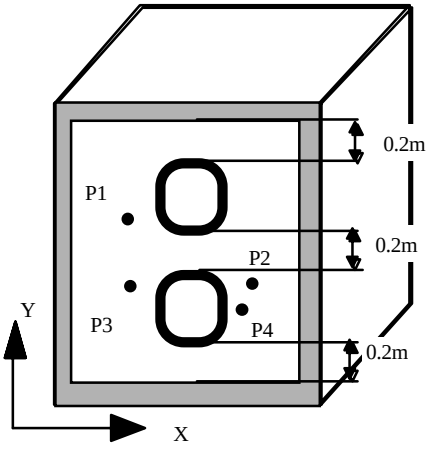

Figure 12. Experiment.

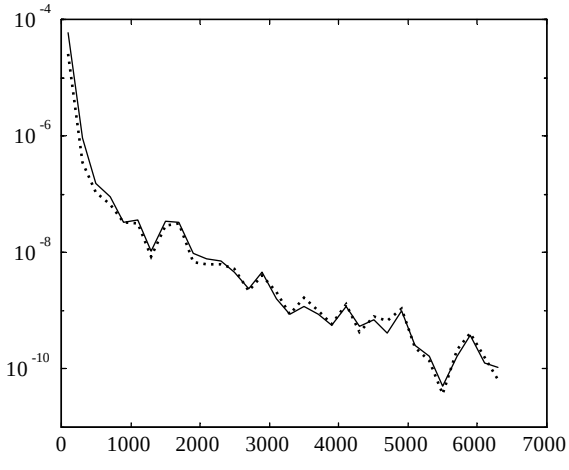

Figure 13. FAQV at the non-excited point P_3 (0·3, 0·48 m) versus frequency; non-correlated sources, bandwidth of calculation 200 Hz. ——, Measurement;……, calculation.

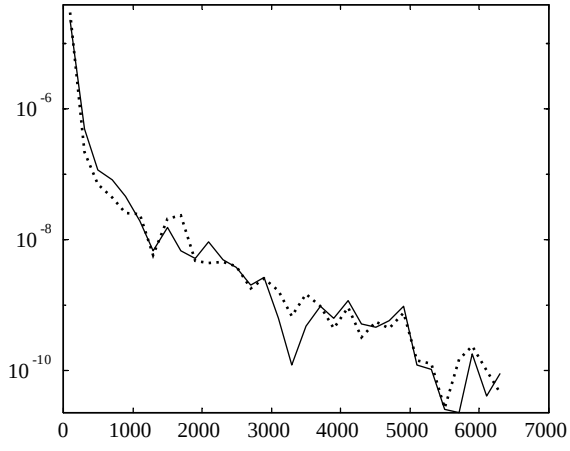

Figure 14. FAQV at the non-excited point P_3 (0·3, 0·48 m) versus frequency; correlated sources, bandwidth of calculation 200 Hz. ——, Measurement;……, calculation.

Correlated forces: the same input signal was provided to both shakers. Consequently, the two driving forces are strongly correlated. The comparison of measured FAQV and calculation with EMo is excellent in the entire frequency range. Figure 14 presents the results at point P_3. As one can see, the agreement is excellent in the entire frequency range demonstrating the validity of the method, even if the forces are correlated.

6. RIGID COUPLING OF TWO SUBSTRUCTURES

In this section one deals with coupled substructures, and the possibility of predicting the global structure behaviour from the knowledge of EMo of substructures. The basic idea is to use the same methodology as in the classic mobility approach, making an analogy between frequency averaged quadratic velocity (FAQV) and pure tone velocity, frequency averaged exchange power (FAP) and coupling force, energy mobility (EMo) and classic mobility. The coupling between substructures is characterized through energy connectivity. Once again, in analogy with classic mobility, that assumes the continuity of displacements and equilibrium of forces at coupling points, one can verify at each coupling point the equality of FAQV and the balance of FAP.

6.1. EXACT CONNECTIVITY BY CLASSIC MOBILITIES

Let us consider two vibrating subsystems S_1 and S_2. Subsystem S_1 is excited at point n by an external force F_n, subsystem S_2 is not directly excited.

The velocity at a point p on S_1, and the velocity at a point m on S_2 after coupling the two substructures S_1 and S_2 at a point c can be obtained, as done in section 3, by using the classic mobilities of the separate substructures. One gets the following coupling force F_c^1:

$$F_c^1 = -\frac{Y_{cn}^1}{Y_{cc}^1 + Y_{cc}^1} F_n^1. \tag{25}$$

After coupling S_1 and S_2, the transfer mobilities on the assembly, between point m or p and point n can be expressed as functions of the mobilities before coupling:

$$Y_{pn} = Y^1_{pn} - (Y^1_{pc} Y^1_{cn})/(Y^1_{cc} + Y^2_{cc}), \tag{26}$$

$$Y_{mn} = (Y^2_{mc} Y^1_{cn})/(Y^1_{cc} + Y^2_{cc}), \tag{27}$$

where Y indicates the mobility of the global system and Y^i the mobility of uncoupled subsystems.

6.2. ENERGY CONNECTIVITY

Let us consider the two subsystems before assembling them. The formalism presented below for EMo is exactly the same as that used for classic mobility calculations. We have to replace in the calculations the pure tone forces by FAP, the velocities by FAQV, and classic mobilities by EMo.

The FAQV at point n on S_1, respectively, at point m on S_2, when S_1 is excited at point n, can be calculated according to the results given in section 3, using the EMo defined in equation (10) as follows:

$$\langle |V^1_n|^2 \rangle = H^1_{nn} \langle \Pi^1_n \rangle, \tag{28}$$

$$\langle |V^2_m|^2 \rangle = 0. \tag{29}$$

Let us now study the behaviour of the structure obtained by coupling the two subsystems at one point c. This point is noted c_1 on subsystem S_1 and c_2 on subsystem S_2. Assuming rigid connection, one has to verify the equality of FAQV at coupling point $c = c_1 = c_2$, and the power flow balance for non-dissipative coupling:

$$\langle |V^1_{c_1}|^2 \rangle = \langle |V^2_{c_2}|^2 \rangle, \tag{30}$$

$$\langle |\Pi^1_{c_1}|^2 \rangle = -\langle |\Pi^2_{c_2}|^2 \rangle. \tag{31}$$

Here $\langle |\Pi^1_{c_1}|^2 \rangle$ (resp. $\langle |\Pi^2_{c_2}|^2 \rangle$) is the FAP at coupling point c, flowing in substructure S_1 (resp. S_2). Using the energy additivity for each subsystem, we can calculate FAQV on S_1 and on S_2 with equations (32) and (33):

$$\langle |V^1_p|^2 \rangle \approx H^1_{pn} \langle \Pi^1_n \rangle + H^1_{pc} \langle \Pi^1_c \rangle, \tag{32}$$

$$\langle |V^2_m|^2 \rangle \approx H^2_{mc} \langle \Pi^2_c \rangle. \tag{33}$$

These relations, written for $m = c$ and $p = c$, can be used in connection with coupling conditions (30) and (31) to calculate the power Π_c exchanged at the coupling point c. One gets the final expression

$$\langle \Pi^1_c \rangle = -\langle \Pi^2_c \rangle \approx -\frac{H^1_{cn}}{H^1_{cc} + H^2_{cc}} \langle \Pi^1_n \rangle. \tag{34}$$

The quadratic velocity at any point of both coupled substructures can then be calculated from the power injected externally, by using equation (34) in equations (32) and (33):

$$\langle |V^1_p|^2 \rangle \approx \left(H^1_{pn} - \frac{H^1_{pc} H^1_{cn}}{H^1_{cc} + H^2_{cc}} \right) \langle \Pi^1_n \rangle, \tag{35}$$

$$\langle |V^2_m|^2 \rangle \approx \frac{H^2_{mc} H^1_{cn}}{H^1_{cc} + H^2_{cc}} \langle \Pi^1_n \rangle. \tag{36}$$

One can describe the behaviour after coupling from data on subsystems before coupling. Considering the two coupled structures as a global one, one can use equations (35) and (36) to define the EMo for the global structure. Expressions are different when the FAQV is calculated on the excited substructure S_1 or on the receiving substructure S_2.

For points p and n on S_1, the transfer EMo H_{pn} on the global system can be identified in equation (35):

$$H_{pn} \approx H^1_{pn} - \frac{H^1_{pc} H^1_{cn}}{H^1_{cc} + H^2_{cc}}. \tag{37}$$

For $m \in S_2$, one can identify the transfer EMo on the global system from equation (36):

$$H_{mn} \approx \frac{H^2_{mc} H^1_{cn}}{H^1_{cc} + H^2_{cc}}. \tag{38}$$

For the coupling point c, one can indifferently use both expressions (37) and (38) to obtain the transfer EMo and the input EMo after coupling:

$$H_{cn} = \frac{H^2_{cc} H^1_{cn}}{H^1_{cc} + H^2_{cc}}, \tag{39}$$

$$H_{cc} = \frac{H^2_{cc} H^1_{cc}}{H^1_{cc} + H^2_{cc}}. \tag{40}$$

One can notice a formal equivalence between these expressions and the one obtained with classic mobilities in section 6.1. In reference [9] the case of two structures coupled at one point is studied. Connectivity conditions (30), (31) are also used and lead to the expression (40) written in terms of Frequency Response Function for Power at the coupling point.

6.3. NUMERICAL EXAMPLES

Numerical simulations were done to verify the validity of the method presented in section 6.2 to calculate the EMo of coupled structures from EMo's of uncoupled structures. The EMo of uncoupled subsystems was calculated by using equation (10). The EMo's of coupled structures were calculated by using equations (37)–(39). The classic mobilities for coupled

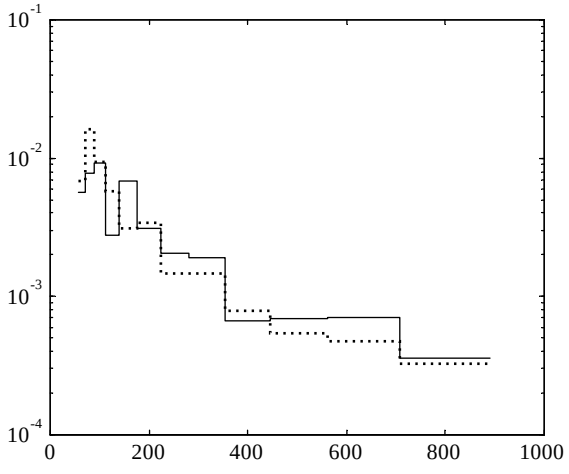

Figure 15. Transfer EMo H_{mn} versus frequency for two identical coupled plates; n (0·5; 0·6) on plate P_1, m (0·5; 0·6) on plate P_2. -------, EMo calculation; ——, exact calculation.

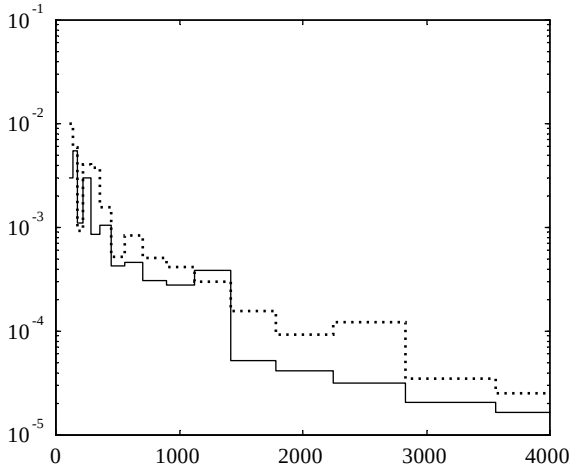

Figure 16. Transfer EMo H_{nm} versus frequency; n (0·5; 0·6) on plate P_1, m (0·5; 0·6) on plate P_3. - - - - - - -, EMo calculation; ——, exact calculation.

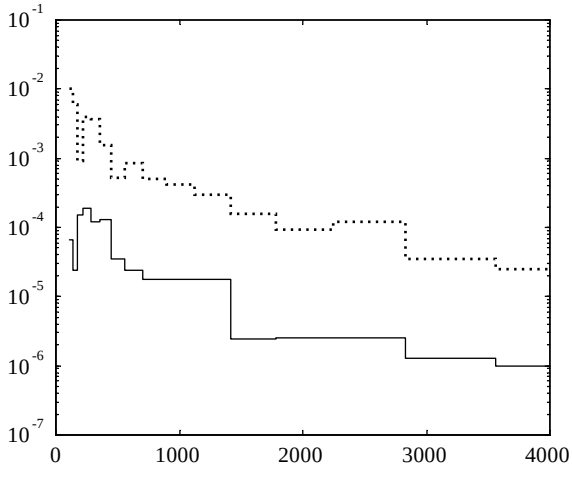

Figure 17. Transfer EMo H_{mn} versus frequency; n (0·5; 0·6) on plate P_1, m (0·5; 0·6) on plate P_3. - - - - - - -, EMo calculation; ——, exact calculation. (a) Exchanged power; (b) FAQV $\langle |V_{c2}|^2 \rangle$.

structures Y_{ij} were calculated by using equations (26) and (27) and introduced in the EMo basic expression (10). This calculation was a reference result for coupled structures to be compared to expressions (37)–(39).

A first calculation was made on an assembly of two identical thin rectangular, simply supported, steel plates. They were connected through three rigid links (see Appendix B: Plates system 1). The transfer EMo between the points n on plate P_1 and m on plate P_2 was calculated with reference expression (10) and expression (38). The comparison presented in Figure 15 demonstrates a good agreement of both calculations.

A second simulation was then performed on an assembly made of the previously used plate P_1 and a plate P_3 a little smaller and thicker than P_1. Once again the plates were connected by three rigid links transmitting only forces (see Appendix B: Plate system 2). The comparison on transfer EMo was surprising; when the thicker plate was excited the agreement of results was correct (see Figure 16), but when the thin plate was excited a large discrepancy was observed, see Figure 17.

6.4. CONCLUSION

The numerical examples presented in Figures 15–17 show that the prediction obtained with EMO is correct only when the mobility of the excited system at the coupling point is not larger than that of the receiving system. In reference [9], one got a good prediction using the frequency response function for power (FRFP) and connectivity conditions (30), (31) in the case of an assembly of two beams of the same material, length and cross-section, coupled at one point. The coupling of different beams was not presented, but one can say, taking into account the explanation given in section 7, that the same discrepancy observed in this paper will occur when using FRFP.

These results showed that the EMo method defined in sections 3 and 6 needed some improvements. This is the aim of the following section.

7. COUPLING OF TWO SUBSTRUCTURES REVISITED

The presentation given in the previous section was unsatisfactory. This section deals with an explanation of this fact. The description of connectivity conditions with equations (30) and (31) is exact for the assumed rigid coupling. We have to conclude that the problem comes from the energy additivity in equations (32) and (33). In section 3, it has been demonstrated that these properties were a good approximation of reality. However, in the present case, the primary force F_n and the coupling force F_c acting on the substructures are completely correlated, so equations (32) and (33) cannot be applied for coupling forces.

7.1. ENERGY ADDITIVITY ON COUPLED STRUCTURES

Let us calculate the quadratic velocity of point p on the excited subsystem (S_1) using equation (1):

$$|V_p^1|^2 = |Y_{pn}^1|^2\ |F_n^1|^2 + |Y_{pc}^1|^2|F_c^1|^2 + 2\mathrm{Re}\{F_n^1 Y_{pn}^1 F_c^{1*}\ Y_{pc}^{1*}\}. \tag{41}$$

The energy additivity (32) was based on the fact that, when averaged over frequency, the cross term of the right member of equation (41), was negligible compared to the other two. For non-particular external loading forces, presented in section 1, this was true, because the cross term fluctuated about zero with frequency. Let us have a look at the present case of coupling forces. Using equation (25), one can write the cross term of equation (41) as follows:

$$2\mathrm{Re}\{F_n^1 Y_{pn}^1 F_c^{1*} Y_{pc}^{1*} = -2\mathrm{Re}\left\{|F_n^1|^2\ \frac{Y_{pn}^1 Y_{pc}^{1*} Y_{cn}^{1*}}{Y_{cc}^{1*} + Y_{cc}^{2*}}\right\}. \tag{42}$$

In general, the cross term is fluctuating with frequency, and thus energy additivity is valid. However, if the quadratic velocity is calculated at the coupling point, one has:

$$2\mathrm{Re}\{F_n^1 Y_{cn}^1 F_c^{1*} Y_{cc}^{1*}\} = -2\mathrm{Re}\left\{|F_n^1|^2|Y_{cn}^1|^2\ \frac{Y_{cc}^{1*}}{Y_{cc}^{1*} + Y_{cc}^{2*}}\right\} \tag{43}$$

$$= -2\,\frac{|F_n^1|^2|Y_{cn}^1|^2|Y_{cc}^1|^2}{|Y_{cc}^1 + Y_{cc}^2|^2} - 2\,\frac{|F_n^1|^2|Y_{cn}^1|^2}{|Y_{cc}^1 + Y_{cc}^2|^2}\,\mathrm{Re}\{Y_{cc}^1\}\ \mathrm{Re}\{Y_{cc}^2\} - 2\,\frac{|F_n^1|^2|Y_{cn}^1|^2}{|Y_{cc}^1 + Y_{cc}^2|^2}\,\mathrm{Im}\{Y_{cc}^1\}\ \mathrm{Im}\{Y_{cc}^2\}. \tag{44}$$

The third term of the right member of equation (44) is in general fluctuating because of $\mathrm{Im}\{Y^1_{cc}\}$ and $\mathrm{Im}\{Y^2_{cc}\}$ (this is not true in the particular case of two identical subsystems coupled at symmetrical points), but the first and second ones are strictly negative and frequency averaging cannot make them negligible. As a consequence, energy additivity (32) is not true at the coupling point, where an additional contribution exists because of cross terms being non-negligible in equation (41).

Energy additivity remains valid at every point far from the coupling point, but it does not work at the coupling point. This is fundamental, because the calculation of the power exchanged at the coupling point is based on the energy additivity at this point. Thus, the exchanged power calculated by assuming energy additivity at the coupling point leads to the discrepancy observed in section 6.

In addition, because the energy additivity remains valid for points different from the coupling point, a good approximation of the FAQV will be obtained for all points different from the coupling points with equation (32) or (33) using a good approximation of the FAP exchanged at the coupling point.

Thus, the basic problem in applying the method is to properly calculate the FAP exchanged at the coupling point.

7.2. CALCULATION OF THE POWER INJECTED AT THE COUPLING POINT

The injected power at the coupling point of substructure S_1 can be exactly calculated at each frequency, using classic mobility, as:

$$\Pi^1_c = \mathrm{Re}\{V^1_c F^{1*}_c\}. \tag{45}$$

The coupled velocity is calculated with equation (2), the effect of the input force F^1_n and the coupling force F^1_c given by equation (25) are added:

$$\Pi^1_c = -\mathrm{Re}\{Y^2_{cc}\}\frac{|Y^1_{cn}|^2}{|Y^1_{cc}+Y^2_{cc}|^2}|F^1_n|^2. \tag{46}$$

Making a frequency average of equation (46) and assuming statistical independence of the frequency distribution of driving force, transfer mobility Y_{cn} and $\mathrm{Re}\{Y^2_{cc}\}/|Y^1_{cc}+Y^2_{cc}|^2$, allows one to get

$$\langle \Pi^1_c \rangle \approx -\langle |Y^1_{cn}|^2 \rangle \langle |F^1_n|^2 \rangle \left\langle \frac{\mathrm{Re}\{Y^2_{cc}\}}{|Y^1_{cc}+Y^2_{cc}|^2} \right\rangle. \tag{47}$$

Equation (47) can be transformed as follows; where one recognizes the EMo and the FAP injected at point n:

$$\langle \Pi^1_c \rangle \approx -\frac{\langle |Y^1_{cn}|^2 \rangle}{\langle \mathrm{Re}\{Y^1_{nn}\} \rangle} \langle |F^1_n|^2 \rangle \langle \mathrm{Re}\{Y^1_{nn}\} \rangle \left\langle \frac{\mathrm{Re}\{Y^2_{cc}\}}{|Y^1_{cc}+Y^2_{cc}|^2} \right\rangle. \tag{48}$$

Finally, the FAP exchanged at coupling point can be written as

$$\langle \Pi^1_c \rangle \approx -H^1_{cn} \langle \Pi^1_n \rangle \left\langle \frac{\mathrm{Re}\{Y^2_{cc}\}}{|Y^1_{cc}+Y^2_{cc}|^2} \right\rangle. \tag{49}$$

In equation (49) it has been assumed that the FAP injected at point n is given by equation (9) as

$$\langle \Pi_n^1 \rangle \approx \langle |F_n^1|^2 \rangle \langle \mathrm{Re}\{Y_{nn}^1\} \rangle.$$

That is to say that the averaged real part of the input mobility at the driving point is not modified by coupling. This is of course an approximation. The exact real part of the input mobility, when coupling is achieved, is given by

$$\mathrm{Re}\{Y_{nn}\} = \mathrm{Re}\{Y_{nn}^1\} - \mathrm{Re}\{Y_{nc}^1 Y_{cn}^1/(Y_{nn}^1 + Y_{nn}^1)\}. \tag{50}$$

However, when taking an average over frequency, the second term tends to be negligible compared to the first one because $\mathrm{Re}\{Y_{nn}^1\}$ is positive contrary to the other term of equation (50), which fluctuates with frequency. Equation (49) is thus a realistic approximation for power exchanged by coupling.

7.3. THE CONNECTIVITY FACTOR

Equation (34) relates the FAP injected at the excitation point n to the FAP exchanged at the coupling point. Equation (49) presents the same relation when the exchanged power is exactly calculated at each frequency and then averaged. It is clear that the expressions are different. This difference can be represented by a connectivity factor introduced into equation (49), in the following way:

$$\langle \Pi_c^1 \rangle \approx -\frac{H_{cn}^1}{H_{cc}^1 + H_{cc}^2} \alpha_c^{12} \langle \Pi_n^1 \rangle, \tag{51}$$

where

$$\alpha_c^{12} = -(H_{cc}^1 + H_{cc}^2) \left\langle \frac{\mathrm{Re}\{Y_{cc}^2\}}{|Y_{cc}^1 + Y_{cc}^2|^2} \right\rangle. \tag{52}$$

Equation (51) can then be transformed in the form

$$-H_{cc}^2 \langle \Pi_c^1 \rangle \approx H_{cc}^1 \langle \Pi_c^1 \rangle + H_{cn}^1 \alpha_{cn}^{12} \langle \Pi_n^1 \rangle. \tag{53}$$

One can recognize in the left member of the equation the expression of the FAQV of point c calculated in the receiving subsystem:

$$\langle |V_c^2|^2 \rangle \approx -H_{cc}^2 \langle \Pi_c^1 \rangle \tag{54}$$

and in the right member of the equation, a modified expression for the energy additivity specific to the coupling point of the excited substructure:

$$\langle |V_c^1|^2 \rangle \approx H_{cc}^1 \langle \Pi_c^1 \rangle + H_{cn}^1 \alpha_{cn}^{12} \langle \Pi_n^1 \rangle. \tag{55}$$

Finally, the EMo method presented in section 3 can be used, if the transfer mobility from an excited point to a coupled point is modified by the connectivity factor. One can use the formalism developed in section 3 in total analogy with the classic mobility if one introduces the modified EMo given by

$$H_{ij}^k = \frac{\langle |Y_{ij}^k|^2 \rangle}{\langle \mathrm{Re}\{Y_{jj}^k\} \rangle} \alpha_{ij}^{kr}. \tag{56}$$

The connectivity factor α_{ij}^{kr} depends on the point i where the FAQV is observed and j where FAP is injected and of the coupled structures k and r. To generalize this expression to all cases one can introduce connectivity factors having the following values: $\alpha_{ij}^{kr} = 1$ if point i is not a coupling point; if point i is a coupling point of substructures k and r, α_{ij}^{kr} is given by equation (52). However, if $i = j$, the connectivity factor reduces to unity ($\alpha_{ii}^{kr} = 1$) (see Appendix A). In other words, if the external power is directly injected at the coupling point, there is no correction and the basic EMo H_{cn}^{i} can be applied.

The physical significance of the connectivity factor based on limiting cases can be given. If the classic input mobility of coupling point for the receiving system is equal to zero (blocked point) or tends to infinity (free point), the actual power exchanged through coupling is zero (see equation (45)). Using EMo without connectivity factor (equation (32)) to calculate the exchanged power leads to the results

$$\textit{for blocked point}: H_{cc}^{2} = 0 \quad \text{and} \quad \langle \Pi_c^1 \rangle = -\langle \Pi_n^1 \rangle, \tag{57}$$

$$\textit{for free point}: \qquad H_{cc}^{2} \gg H_{cc}^{1} \quad \text{and} \quad \langle \Pi_c^1 \rangle = 0. \tag{58}$$

The exchanged power is not equal to 0 when the receiving structure has low mobility and thus, blocks the coupling point of the excited system. This explains the discrepancy observed in Figures 16 and 17.

On the contrary, by introducing the connectivity factor, namely, using equations (51) and (52), the following results can be obtained:

$$\textit{for blocked point}: H_{cc}^{2} = 0, \quad \alpha_{cn}^{12} = 0 \quad \text{and} \quad \langle \Pi_c^1 \rangle = 0, \tag{59}$$

$$\textit{for free point}: \qquad H_{cc}^{2} \gg H_{cc}^{1}, \quad \alpha_{cn}^{12} = 1 \quad \text{and} \quad \langle \Pi_c^1 \rangle = 0. \tag{60}$$

The coupling FAP is equal to zero as expected. Then using equation (55) one gets:

$$\textit{for blocked coupling point}: \langle |V_c^1|^2 \rangle = 0, \tag{61}$$

$$\textit{for free coupling point}: \qquad \langle |V_c^1|^2 \rangle = H_{cn}^{1} \langle \Pi_n^1 \rangle. \tag{62}$$

Results are now in agreement with reality; for a blocked coupling point the FAQV is zero, and for a free coupling point the FAQV is equal to the uncoupled value. In the following, the definition (56) is used for the EMo.

7.4. NUMERICAL RESULTS USING ENERGY MOBILITY

Two assemblies of plates are studied: the plate system 2 made of two thin homogeneous plates, and the plate system 3 obtained by adding some mass heterogeneities on one of the two plates used in the plate system 2. The results on FAQV at several points and FAP exchanged at coupling points are presented. The exact calculation with classic mobilities serves as a reference to compare with prediction using EMo. Equation (56) is used to calculate EMo of each plate, equation (37) gives the transfer EMo of coupled plates, equations (35) and (36) give the FAQV, and finally equation (34) gives the FAP exchanged at coupling points.

7.4.1. *Assembly of two homogeneous plates*

Let us consider the plate system 2. FAP and FAQV at a coupling point are shown in Figure 18. For FAQV one can see that the EMo calculation matches well the exact prediction, the difference between the two curves in Figure 18(b) being less than 3 dB. For FAP (see Figure 18(a)) the difference between exact prediction and EMo calculation is also

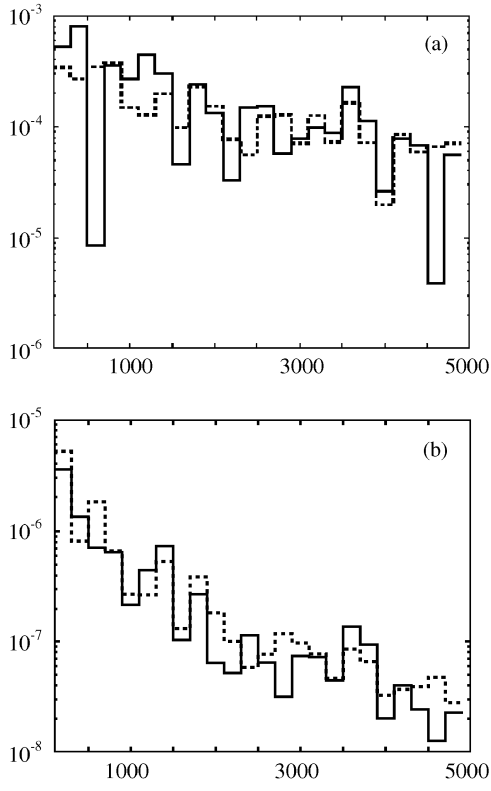

Figure 18. Comparison between exact and EMo calculation at the coupling point c_2 (0·4, 0·2). - - - - - - -, EMo calculation; ——, exact calculation.

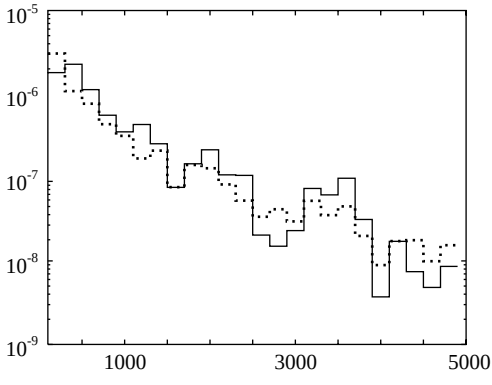

Figure 19. FAQV at the uncoupled point m (0·5, 0·6) versus frequency. - - - - - - -, EMo calculation; ——, exact calculation. (a) Exchanged power; (b) FAQV.

less than 3 dB except for two dips in the exact calculation, at 500 and 4500 Hz, which are not visible in the EMo calculation. These dips tend to disappear when the width of the frequency band increases. However, these differences on the FAP have only a little influence on the FAQV, demonstrating that FAQV prediction is more robust than FAP prediction.

The result for FAQV at one uncoupled point is presented in Figure 19; agreement is quite good. This case previously treated using EMo without the connectivity factor,

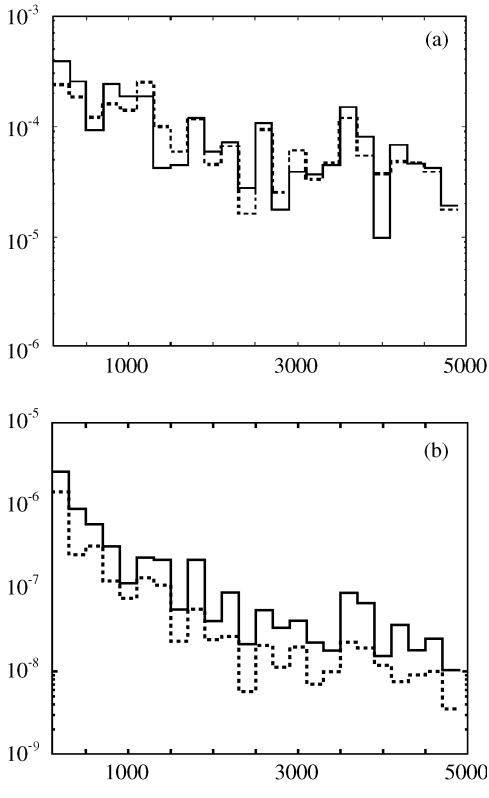

Figure 20. Comparison between exact and EMo calculations at c_2 (0·4, 0·2); plate P_1 heterogeneous. - - - - - - -, EMo calculation; ——, exact calculation.

led to discrepancy (see Figure 17) and demonstrates the importance of the connectivity factor.

7.4.2. *Assembly of two heterogeneous plates*

Plate system 2 is modified by adding point masses, as described in Appendix B (plate system 3). Comparison of FAP and FAQV calculated with EMo and exact calculation are presented in Figures 20 and 21. A good agreement is noted at all the tested points: coupling point, uncoupled point and point of heterogeneity. Compared to the results from homogeneous plates, the agreement of exact prediction and EMo calculation for heterogeneous plates is of the same quality.

8. CONCLUSIONS

The energy mobility (EMo) method has been presented and used to predict the frequency averaged quadratic velocity of coupled plates excited by broadband point sources. The method is based on approximations assuming statistical independence between frequency distributions of force and mobilities spectra. The method can be used to calculate point frequency averaged quadratic velocities (FAQV) from point frequency averaged injected power (FAP). No phase information between the loads is needed. A general energy connectivity allows us to predict FAQV and FAP, on an assembly, as functions of the EMo of uncoupled substructures and of injected FAP.

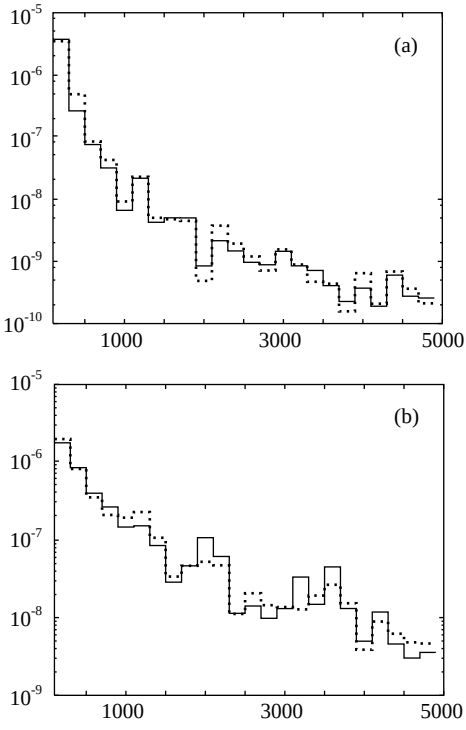

Figure 21. FAQV versus frequency on the heterogeneous plate system 3. (a) FAQV at the heterogeneity point n (0·5, 0·6) on plate P_1; (b) FAQV at point m (0·5, 0·6) on plate P_3. - - - - - - -, EMo calculation; ——, exact calculation.

The validity of the approach has been demonstrated, for one isolated plate in the medium-frequency range, first by numerical simulation and then experimentally. Good results are observed even in the case of totally correlated forces. The approximation tends asymptotically to the exact calculation when the averaging frequency bandwidth increases. An error <3 dB was observed in the typical case of averaging frequency bands of 200 Hz, plate modal density of 0·2 modes/Hz and damping loss factor of 0·01.

The EMo concept seems very interesting regarding industrial structures because it has been observed that, contrary to classic mobility, it is insensitive to mass heterogeneities located at excitation points. This will reduce the sensitivity of prediction to heterogeneity uncertainty that appears with classic calculation technique.

The fundamental interest in the EMo method is due to the possibility, in analogy with the classic mobility method, of predicting FAQV of coupled subsystems from the knowledge of EMo of uncoupled subsystems. However, contrary to classic mobilities, it is necessary to introduce a connectivity factor. Because its ingredients are the classic mobilities, which can furthermore be measured on industrial systems, the method has straightforward experimental applications.

ACKNOWLEDGMENTS

This work was supported by EDF (Electricité de France) - DER Clamart, and INRS (Institut National de Recherche sur la Sécurité) - MAV, Vandoeuvre, France. In particular, we wish to thank E. Luzzato and T. Loyau for their kind suggestions.

REFERENCES

1. J. PLUNT 1996 *Proceedings of Internoise'96, Liverpool* Vol. **6**, 3047–3051. Generic limitations of vibro-acoustic prediction methods for product noise.
2. R. J. BERNHARD 1996 *Proceedings of Internoise'96, Liverpool* Vol. **6**, 2867–2872. The limits of predictability due to manufacturing and environmentally induced uncertainty.
3. L. CREMER, M. HECKL and E. E. UNGAR, 1973 *Structure Borne Sound*. Berlin: Springer Verlag.
4. R. S. LANGLEY 1990 *Journal of Sound and Vibrations* **141**, 207–219. A derivation of the coupling loss factors used in statistical energy analysis.
5. J. E. MANNING 1994 *Philosophical Transactions of the Royal Society of London* **A346**, 477–488. Formulation of SEA parameters using mobility functions.
6. C. CACCIOLATI and J. L. GUYADER 1994 *Philosophical Transactions of the Royal Society of London* **A346**, 465–475. Measurement of SEA coupling loss factors using point mobilities.
7. K. SHANKAR and A. J. KEANE 1995 *Journal of Sound and Vibration* **181**, 801–838. A study of the vibrational energies of two coupled beams by finite element and Green function (receptance) methods.
8. XU WANG and L. L. KOSS 1995 *Journal of Sound and Vibration* **155**, 55–73. Frequency response functions for power, power transfer ratio and coherence.
9. L. L. KOSS 1995 *Journal of Sound and Vibration* **181**, 709–725. Frequency response functions for power and connectivity.
10. O. M. BOUTHIER and R. J. BERNHARD 1992 *American Institute of Aeronautics and Astronautics Journal* **30**, 616–623. Models of space averaged energetics of plates.
11. R. LANGLEY 1994 *Journal of Sound and Vibration* **178**, 483–500. Spatially averaged frequency response envelopes for one- and two-dimensional structural components.
12. J. M. MONDOT and B. PETERSSON 1987 *Journal of Sound and Vibration* **114**, 507–518. Characterization of structure-borne sound sources: the source descriptor and the coupling function.
13. M. R. SCHROEDER 1969 *Journal of the Acoustical Society of America* **46**, 277–283. Effect of frequency and space averaging on the transmission responses of multimodal media.
14. A. GIRARD and H. DEFOSSE 1990 *Journal of Sound and Vibration* **137**, 53–68. Frequency response smoothing, matrix assembly and structural paths: a new approach for structural dynamics up to high frequencies.
15. R. G. DEJONG 1992 *Proceedings of Internoise '96, Liverpool* Vol. **6**, 2885–2890. Statistical measures of the response functions of simple and complex structures.
16. E. SKUDRZYK 1980 *Journal of the Acoustical Society of America* **67**, 1105–1135. The mean-value method of predicting the dynamic response of complex vibrators.
17. J. O'HARA 1967 *Journal of the Acoustical Society of America* **41**, 1180–1184. Mechanical impedance and mobility concepts.
18. S. MAHALINGAM 1975 *Journal of Sound and Vibration* **40**, 337–350. The synthesis of vibrating systems by use of internal harmonic receptances.
19. V. I. POPKOV 1975 *Vibroacoustic Diagnostics and Reduction of the Shipboard Machinery* (translated from Russian). Arlington, VA: Join Publications Research Service.

APPENDIX A: CASE OF EXCITED COUPLING POINT

In section 3 the power injected at the coupling point between substructures was calculated. The excited point n was considered far from coupling points c. In this case the injected power does not vary with coupling; it was calculated using equation (9). Equations (44) and (55) have shown that the velocity V_c varies strongly with coupling and the power flow at the coupling point depends on the connectivity factor which was not equal to unity. Let us now consider the case of a directly excited coupling point shown in Figure A1. In this case the classical input mobility and the injected power vary strongly with coupling.

The input mobility at the coupling point on the assembly is

$$Y_{cc} = \frac{Y^1_{cc} Y^2_{cc}}{Y^1_{cc} + Y^2_{cc}}, \tag{A1}$$

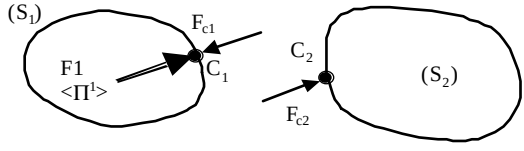

Figure A1. Excited coupling point.

and the frequency averaged power injected by the input force F_1 is

$$\langle \Pi^1 \rangle = \tfrac{1}{2} \langle \mathrm{Re}\{Y_{cc}\} |F_1|^2 \rangle. \tag{A2}$$

Equation (A1) is used in equation (A2). As in the other parts of the paper, the averaged product of positive functions is approximated as the product of averaged positive functions:

$$\langle \Pi^1 \rangle = \frac{1}{2} \left\langle \frac{|F_1|^2}{|Y^1_{cc} + Y^2_{cc}|^2} \right\rangle [\langle \mathrm{Re}\{Y^1_{cc}\} |Y^2_{cc}|^2 \rangle + \langle \mathrm{Re}\{Y^2_{cc}\} |Y^1_{cc}|^2 \rangle]. \tag{A3}$$

The coupling force between the subsystems is

$$F^1_c = -\frac{Y^1_{cc}}{Y^1_{cc} + Y^2_{cc}} F_1, \tag{A4}$$

and the coupling FAP between the subsystems given in equation (A5) was also approximated (see equation (A6).):

$$\langle \Pi^1_c \rangle = \tfrac{1}{2} \langle V_c F^{1*}_c \rangle = \tfrac{1}{2} \langle Y_{cc} F_1 F^{1*}_c \rangle, \tag{A5}$$

$$\langle \Pi^1_c \rangle \approx -\frac{1}{2} \left\langle \frac{|F_1|^2}{|Y^1_{cc} + Y^2_{cc}|^2} \right\rangle \langle \mathrm{Re}\{Y^2_{cc}\} |Y^1_{cc}|^2 \rangle. \tag{A6}$$

The ratio of the coupling FAP on the injected FAP is shown in equations (A7) and (A8). To introduce the EMo, the numerator and the denominator were divided by the product of the real parts: $\mathrm{Re}\{Y^1_{cc}\}\ \mathrm{Re}\{Y^2_{cc}\}$:

$$\frac{\langle \Pi^1_c \rangle}{\langle \Pi^1 \rangle} = -\frac{\langle \mathrm{Re}\{Y^2_{cc}\} |Y^1_{cc}|^2 \rangle}{\langle \mathrm{Re}\{Y^1_{cc}\} |Y^2_{cc}|^2 + \langle \mathrm{Re}\{Y^2_{cc}\} |Y^1_{cc}|^2 \rangle} \tag{A7}$$

$$\approx -\frac{\langle \mathrm{Re}\{Y^2_{cc}\} \rangle \langle |Y^1_{cc}|^2 \rangle}{\langle \mathrm{Re}\{Y^1_{cc}\} \rangle \langle |Y^2_{cc}|^2 \rangle + \langle \mathrm{Re}\{Y^2_{cc}\} \rangle \langle |Y^1_{cc}|^2 \rangle}, \tag{A8}$$

$$\langle \Pi^1_c \rangle \approx -\frac{\dfrac{\langle |Y^1_{cc}|^2 \rangle}{\langle \mathrm{Re}\{Y^1_{cc}\} \rangle}}{\dfrac{\langle |Y^1_{cc}|^2 \rangle}{\langle \mathrm{Re}\{Y^1_{cc}\} \rangle} + \dfrac{\langle |Y^2_{cc}|^2 \rangle}{\langle \mathrm{Re}\{Y^2_{cc}\} \rangle}} \langle \Pi^1 \rangle. \tag{A9}$$

Finally, the following equation is obtained, and compared to equation (51). This comparison shows that in this particular case the connectivity factor is unity:

$$\langle \Pi^1_c \rangle = -\frac{H^1_{cc}}{H^1_{cc} + H^1_{cc}} \langle \Pi^1 \rangle. \tag{A10}$$

APPENDIX B: DESCRIPTION OF SYSTEMS
(the locations of points are given in meters)

Plate system 1
Plates P_1 and P_2: dimensions: $Lx = 1{\cdot}0$ m, $Ly = 0{\cdot}7$ m, $h = 0{\cdot}001$ m;
material: $\rho = 7800\ \text{kg/m}^3$, $E = 2{\cdot}1 \times 10^{11}$ Pa, $v = 0{\cdot}33$, $\eta = 0{\cdot}01$;
connection points (the same on both plates): $c_1(0{\cdot}2\,;0{\cdot}5)$, $c_2(0{\cdot}4\,;0{\cdot}2)$, $c_3(0{\cdot}7\,;0{\cdot}3)$;
studied points: $n(0{\cdot}5\,;0{\cdot}6)$ on plate P_1, $m(0{\cdot}5\,;0{\cdot}6)$ on plate P_2.

Plate system 2
Plate P_1: dimensions: $Lx = 1{\cdot}0$ m, $Ly = 0{\cdot}7$ m, $h = 0{\cdot}001$ m; Plate P_3: dimensions: $Lx = 0{\cdot}9$ m, $Ly = 0{\cdot}7$ m, $h = 0{\cdot}004$ m; material: $\rho = 7800\ \text{kg/m}^3$, $E = 2{\cdot}1 \times 10^{11}$ Pa, $v = 0{\cdot}33$, $\eta = 0{\cdot}01$;
connection points (the same on both plates): $c_1(0{\cdot}2\,;0{\cdot}5)$, $c_2(0{\cdot}4\,;0{\cdot}2)$, $c_3(0{\cdot}7\,;0{\cdot}3)$;
studied points: $n(0{\cdot}5\,;0{\cdot}6)$ on plate P_1, $m(0{\cdot}5\,;0{\cdot}6)$ on plate P_3.

Plate system 3
Plate P_1: dimensions: $Lx = 1{\cdot}0$ m, $Ly = 0{\cdot}7$ m, $h = 0{\cdot}001$ m;
Plate P_3: dimensions: $Lx = 0{\cdot}9$ m, $Ly = 0{\cdot}7$ m, $h = 0{\cdot}004$ m; material: $\rho = 7800\ \text{kg/m}^3$, $E = 2{\cdot}1 \times 10^{11}$ Pa, $v = 0{\cdot}33$, $\eta = 0{\cdot}01$;
coupling points (the same on both plates): $c_1(0{\cdot}2\,;0{\cdot}5)$, $c_2(0{\cdot}4\,;0{\cdot}2)$, $c_3(0{\cdot}7\,;0{\cdot}3)$;
excited points on P_1: $n_1(0{\cdot}4\,;0{\cdot}4)$, $n_2(0{\cdot}5\,;0{\cdot}6)$ by constant unit loading forces $Fe = 1$ N; with point attached masses on plate P_1; 0·1 kg at point $c_1(0{\cdot}2\,;0{\cdot}5)$, 0·2 kg at point $n_2(0{\cdot}5\,;0{\cdot}6)$ and 0·5 kg at point $n_3(0{\cdot}6\,;0{\cdot}3)$.
studied points: $n = n_2$ on plate P_1, m $(0{\cdot}5\,;0{\cdot}6)$ on plate P_3.